Prediction of Base Pressure Using Semi-Analytical Model For Multi-Nozzle Cluster

A thesis submitted in the partial fulfilment of the requirements of the degree of

Master of Technology

by
Mani Shankar Yadav
(193012003)

Supervisor:
Prof. Krishnendu Sinha

Department of Aerospace Engineering
Indian Institute of Technology Bombay
Mumbai (400 076), India
June 2021

Acceptance Certificate

Department of Aerospace Engineering
Indian Institute of Technology Bombay

The M.Tech. project report entitled "Prediction of Base Pressure Using Semi-Analytical Model For Multi-Nozzle Cluster" submitted by Mani Shankar Yadav (roll no. 193012003) may be accepted for being evaluated.

Date: 12-Jul-2021

Digital Signature
Krishnendu Sinha (i06005)
12-Jul-21 12:06:28 PM

Prof. Krishnendu Sinha

Approval Sheet

This thesis entitled "Prediction of Base Pressure Using Semi-Analytical Model For Multi-Nozzle Cluster" by Mani Shankar Yadav is approved for the degree of Master of Technology.

Examiners:

Digital Signature
Abhijit Gogulapati (10001852)
12-Jul-21 03:12:23 PM
. . . .

Digital Signature
Debasis Chakraborty (20001833)
12-Jul-21 03:56:41 PM
. . . .

Supervisor:

Digital Signature
Krishnendu Sinha (i06005)
12-Jul-21 12:06:44 PM
. . . .

Chairperson:

. . . .

Date: 12-Jul-2021

Place: Online

Declaration

I, the undersigned, hereby declare that I am the sole author of this dissertation. To the best of my knowledge, this dissertation contains no material previously published by any other person except where due acknowledgement has been made and relevant sources have been cited.

Mani

Date:

Mani Shankar Yadav
Roll No. 193012003

Acknowledgement

I would like to thank Prof. Krishnendu Sinha for providing guidance and handholding support while working on the inviscid gas dynamics model. His encouragements were filled with baby steps in approaching the study of multijet interactions.

I would also like to thank Pratikkumar Raje for providing CFD simulation results for post processing, Pankaj Niranjan for suggesting meaningful insights and other members of the Hypersonic CFD lab for their kind support.

Abstract

A common practice to achieve a given thrust level and reduced engine length is to rely on clustering of rocket nozzles. However, this posses a problem of multi-jet interaction at higher altitude because of highly under-expanded jets. The formation of trailing shock wave triggers a reverse flow towards the base known as 'updraft plume'. The impingement of the updraft plume on the rocket base raises concern on base drag, base heating and affects the avionics installed in the base region. The flow associated with multi-jet interaction is complex. So, a simplified 2D analytical model is presented with viscous factors that are obtained from CFD simulations to predict the base pressure at given NPR of a particular configuration. The model utilize the analytical relations for expansion fan, oblique shock waves and isentropic flow process. The semi-analytical model slightly over predicts the pressure at the base centre but the trend is well captured.

Keywords: updraft plume, shock wave, expansion fan, shear layer

List of Figures

List of Tables

List of Symbols

$p_{chamber}$	Chamber pressure
p_j	Static pressure at nozzle exit
p_{infl}	Inflection point pressure
p_∞	Static freestream pressure
p_b	Pressure at rocket base centre
p_s	Static pressure at the tail of expansion fan
p^*	Sonic point pressure
M	Mach number
M_j	Mach number at nozzle exit
M_s	Mach number at the tail of the expansion fan
$M_{s,n}$	Shock normal Mach number ahead of the expansion fan
$M_{s,t}$	Tangential Mach number ahead of the expansion fan
θ_{exp}	Flow deflection angle
β_{shock}	Trailing shock wave angle
γ	Ratio of specific heats
L	Nozzle extension length from base plate
D_b	Rocket base diameter
D_e	Nozzle exit diameter
D_s	Diameter of circle through nozzle centreline
D_s/D_e	Nozzle spacing ratio
L/D_e	Nozzle extension ratio
A/A^*	Local area ratio (AR)

Contents

Chapter 1

Introduction

Multi nozzles are widely used in rockets as it reduces nozzle length (reduction in weight increase in payload) compared to a single nozzle and provides better controllability (individual gimbaling is possible). But the multi-jet comes with a cost of plumes interaction at higher altitude form neighbouring nozzles. We also face a phenomenon known as base buffeting. In May 1991, Swedish Space Corporation's Maxus suborbital rocket mission became a failure because of excessive base heating which burnt the guidance control cables. Similarly, in the year 1958 the base burning of the Jupiter I rocket of US Army caused mission failure.

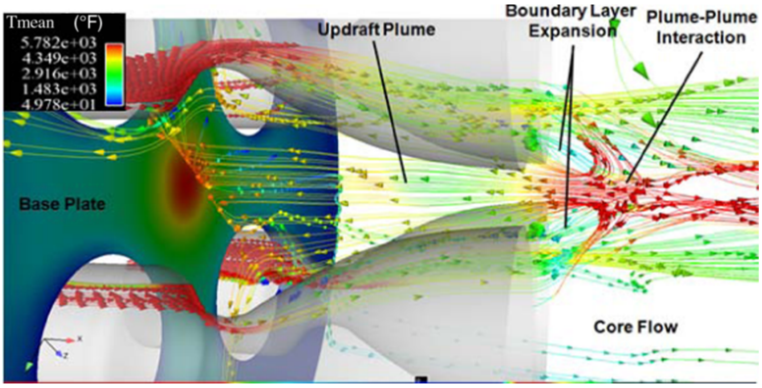

Figure 1.1: Showing base recirculation flow field[3]

During ascent of the multi-nozzle cluster rocket, at lower altitude jets will be over-expanded and they do not interact rather they pull free stream air into the base. This is called aspiration action. As the rocket gains altitude, the jets become under-expanded. The under-expanded jets impinge on one another as they expand radially resulting in the formation of trailing shock wave. Some of the low energy gases will not be able to negotiate the wake pressure rise due to trailing shock wave. A portion of exhaust gases are then turned towards the base known as reverse flow or 'updraft plume' as shown in figure 1.1. At the jets interaction point, a stagnation point exists known as inflection point. There is continuous transfer of mass, momentum and energy towards the base. Consequently, there will be significant increase in base drag and also severe base heating. This can lead to loss of stability and also ineffectiveness of control surfaces (fins) installed near base. The performance of electronic equipment are also compromised. Therefore, it becomes of paramount importance to study the base pressure. The base flow field constitutes of inviscid flow structures like expansion fans and highly viscous regions like shock waves and shear layers. The interactions of the combinations of these viscous and inviscid flow structures make the flow field fairly complex.

1.1 Significance of study

It becomes a paramount importance to study the flow field and should be able to predict the pressure and temperature in the base region. Some of the reasons are mentioned below:

1. The design and development of thermal protection system requires base pressure and temperature data.
2. The data around the base environment can be of great importance for the aerodynamics department so they can reduce drag.
3. The electronic items can be placed at the proper location so that their performance is not compromised.
4. Issue like base buffeting can be understood.[2]

My study is focused on predicting pressure at the base centre of the rocket with four nozzle cluster. In order to predict the base pressure, a 2D inviscid analytical model is proposed by Prof. Krishnendu Sinha. The viscous effects were introduced with the help of CFD simulations performed by Pratikkumar Raje.

Chapter 2

Literature Survey

The flow field of multi jet interaction is quite complex. There has been performed computational as well as experimental work in this field. The computational work seems to be more informative and cost effective over experimental ones.

2.1 Experimental study

Configuration	Nozzle spacing ratio, D_s/D_e	Nozzle extension, in.	Nozzle extension ratio, L/D_e	Nozzle type	Nozzle area ratio, A_e/A_t	General comments
1a	2.18	$5\frac{3}{32}$	1.7326	Bell	12	
1b		$2\frac{1}{16}$	.7015			
1c		$\frac{1}{8}$	.0425			
2	1.67	$4\frac{1}{2}$	1.5306			
3	2.97	2.0	.6803			
4	2.22		.9091	$17\frac{1}{2}^{\circ}$ Conical	6.9	
5	2.18		.6803	Bell	12	Side engines gimbaled 7° downward
6	2.22		.9091	$17\frac{1}{2}^{\circ}$ Conical	6.9	Nitrogen probe installed

Figure 2.1: Various configurations used in experimental study of base heat flux, temperature and pressure[4]

The experiment was performed by Musial and Ward [4] in 1961 at NASA Lewis 10ft. x 10ft. supersonic wind tunnel to examine the base heating problem of four-cluster nozzle configurations at higher Mach numbers (2.0 to 3.5) and nozzle pressure ratio range of 340 to 6800. They used four nozzles cluster for various configurations as shown in figure 2.1. These tests were

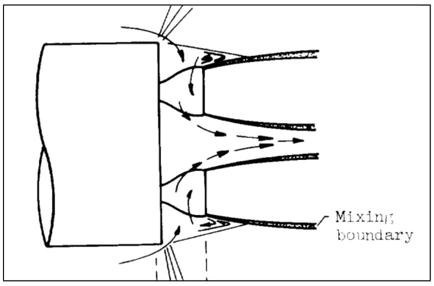

(a) Aspiration flow (low altitude)

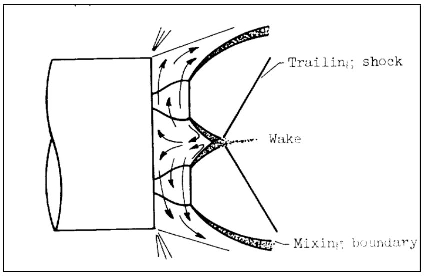

(b) Choked flow (high altitude)

Figure 2.2: Different flow phenomena[4]

performed for bell-shaped and conical nozzles having exit half-angles of 3°and 17.5°with area ratios of 12 and 6.9 respectively. The geometrical parameters like nozzle spacing and nozzle extension were varied during the experiment to study their effects on pressure, temperature and heat flux at rocket base. It was found that the base heat flux within cluster core region decreased as the motor spacing and motor extension increased[4]. The pressure, p/p_∞ was highest at the centre of the cluster and decreased in radial direction.

At lower altitudes, the turbulent mixing boundaries from neighbouring nozzles do not interact. The exhaust jet rather acts as ejectors as they pull air from free-stream to the base causing aspiration action as shown in figure 2.2 (a). As altitude increases the under-expanded plumes impinges on one another. The low energy gases cannot negotiate adverse pressure downstream and start flowing towards the rocket base. After a certain altitude the reverse flow gets choked as shown in figure 2.2 (b) and becomes insensitive to the increase in altitude.

Desikan et al. studied the starting characteristics of under-expanded twin jets and associated reverse flow. Their pressure survey using pitot tube proved the existence of reverse flow due to jet interaction. Expansion fan was observed at the nozzle exit as result of under-expansion of the jets. The important features such as jet core, jet boundary, shear-layer growth, jet shocks and expansion fans at the nozzle exit were captured in Schlieren images. The flow field at NPR $p_j/p_\infty = 90$ is shown in figure 2.3. The reverse flow Mach number for partially under-expanded jets was observed to be subsonic, where as for fully under-expanded jets, the reverse flow was first supersonic while heading towards the base and then turn subsonic as it approached the base. As the NPR increased, the inflection point moved towards the base [1].

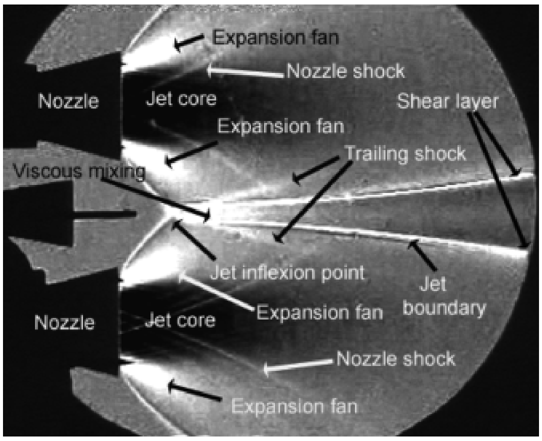

Figure 2.3: Schlieren image showing flow features at $p_j/p_\infty = 90$ for twin under-expanded jets[1]

2.2 Computational study

The computational work by Raje and Sinha[6] throws light on complex flow field by classifying the interactions in various categories. The interactions of shock and expansion fan are regarded as inviscid interactions. The free shear layer interactions and shock come under viscous interactions. The combination of inviscid and viscous interaction is when expansion fan and shear layer interact. The simulations predict similar trend for the base pressure. A multi-grid block consisting of 6.27 millions cells were created to study the flow domain. This study suggests us the challenging task of performing CFD simulations of such a complex flow domain.

The numerical study of multi-jet flow field conducted by Mehta et al. primarily focuses on the multi-species flow field and its effect on base pressure and heating. Plumes interactions at lower and higher altitude are presented. The base heating was found to be sensitive to the nozzle inner wall temperature. The plume induced flow separation (PIFS) is flow structure that is observed during the base recirculating flow regime and partially affects both base heating and base drag. The rocket experiences change in aerodynamic forces and moments due to flow separation occurring at the base.[3]

Nallasamy et al. [5] also has conducted computational study on base pressure and heating. Their simulations showed a qualitative agreement of base pressure and heating with wind tunnel data. There was significant discrepancies between the computed and measured values. These errors were attributed to the ideal gas assumptions and accuracy of turbulence modelling.

[6]

2.3 Need for analytical model

A detailed analytical study of flow field is a challenging task whereas the experimental study requires very sophisticated setup and equipment to conduct experiments. The instrumentation might be subjected to failure due to high temperature of combustion products if we are doing a hot test. Mechanical failures can occur if the vibrations associated with the experiment is not considered well in advance before conducting the experiment. These factors make experimental study a tough task. We cannot deny that the experimental studies are the studies that throws light on the reality and act as the highest benchmark for validation of any model.

The numerical study can come to our rescue. But the computational study comes with its own short comings such as intensive work on grid generation and subsequent requirement of computational time and resources to solve the full Navier-Stokes equations or equations with relevant assumptions like Reynolds Averaged Navier Stokes (RANS) equations. The formulation of RANS equations itself pose a closure problem.

If we simulate the rocket base flow field, we need to vary the ambient conditions. This is because during ascent, the rocket is continuously changing its altitude which results in variation in ambient pressure. So, we need to perform many simulations by varying the inlet conditions of the constructed flow domain in order to know the base pressure. This means doing CFD simulations for various altitudes will be cumbersome. So, CFD simulations may not be a good choice to predict the base pressure at various altitudes.

2.4 Objective of this study

We ask ourselves can we build a model that uses some useful relations from inviscid theory for calculating pressure and perform simulations for extreme test cases so that we can estimate a numerical factor/s that capture/s most of the viscous effects? We do this so that the model can fairly predict the base pressure value at all other intermediate NPRs within the given range without doing a computational intensive simulations. The answer is 'yes' there is a mid way between experiments and CFD.

First of all, we need to identify the primary flow structures like expansion fan and trailing shock wave that has noteworthy impact on the rocket base pressure without missing out the essential flow physics like reverse flow phenomenon. The effect of secondary flow structures can be summed up by using some relevant factors.

For a given NPR range of 990 to 3760 and fixed geometric configuration, a model that utilizes analytical relations related to Prandtl Meyer expansion fan and oblique shock wave can be developed. Simulations are conducted for two NPR cases to come up with factors that can encapsulate the visocous effects like shear layer mixing, jet curvature effect and so on. These two test cases act as lower and upper bounds of NPR in which the model predicts the base pressure satisfactorily. In a nutshell, a model that emphasises on primary flow structures to calculate the pressure at the rocket base centre at different NPRs can be build in association with CFD and is validated against experimental results of Musial and Ward [4].

Chapter 3

Proposed Analytical Model

3.1 Preliminary model

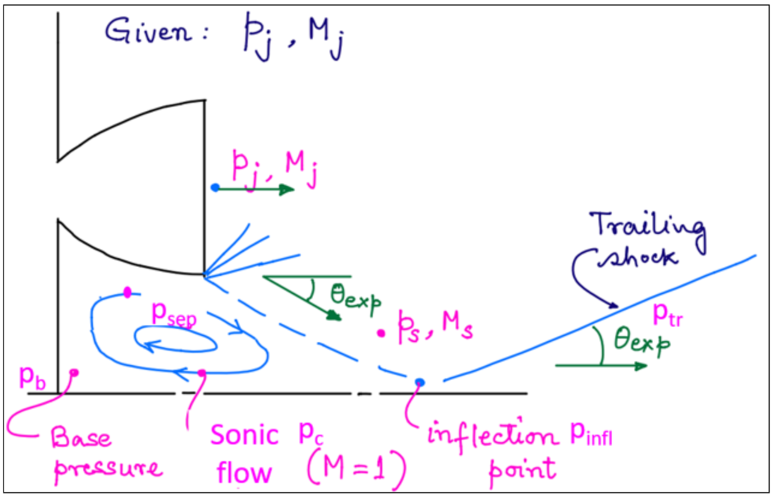

Figure 3.1: Preliminary inviscid 2D analytical model

A simplified analytical model is proposed by Prof. Krishnendu Sinha as base line to study multi-jet interaction as shown in figure 3.1. The model commences with static pressure and Mach number at nozzle exit and calculates pressure at rocket base centre due to reverse flow impingement on the base. The reverse flow phenomenon is triggered because of under-expanded jets interaction at higher altitude forming a trailing shock wave. The model focuses on the reverse flow region between the nozzles cluster near the rocket base.

The model studies taking in consideration of four nozzle cluster without any gimbaling. Due to symmetry of the problem, we only study a quarter of of the flow field as shown in the figure 3.2. The geometric parameters like nozzle spacing ratio, D_s/D_e and nozzle extension ratio, L/D_e play vital role when it comes to base pressure. The base pressure p_b/p_∞ increases if there is decrease in D_s/D_e and L/D_e and vice versa[4].

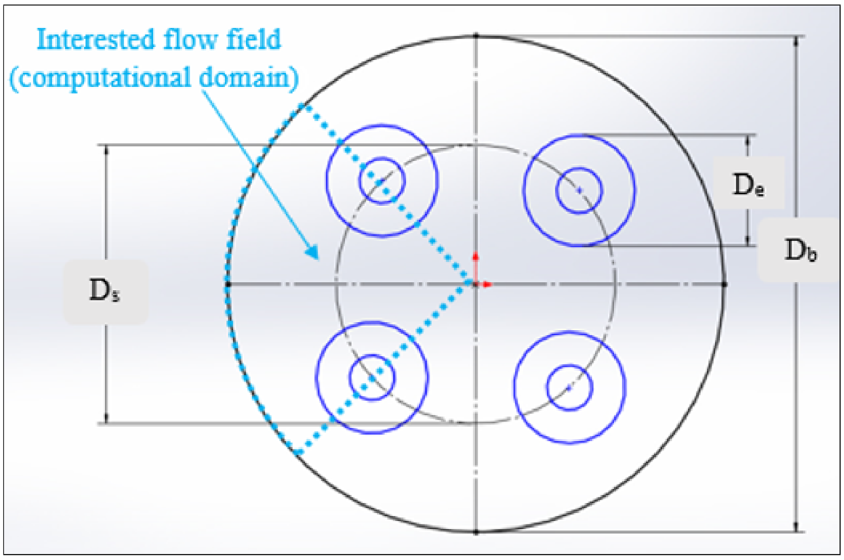

Figure 3.2: Nozzle clustering

3.2 Description of preliminary model

The underexpanded supersonic jet ejecting from the convergent-divergent nozzle undergoes further expansion via expansion fan emanating from the nozzle lip as the flow is deflected away from the main bulk flow. The flow again changes its course by turning on itself via trailing shock. The low energy gases that cannot make their way through the trailing shock wave starts to move towards the base known as 'updraft plume'. The point where plumes from four nozzles meet and the flow stagnates is called inflection point. It lies on the vehicle centreline also called line of symmetry as shown in figure 3.1. The updraft plume then accelerates to Mach 1 reaching sonic point in the flow, undergoes viscous dissipation and stagnates at the rocket base.

3.3 Assumptions of preliminary model

1. It is a two dimensional model with supersonic flow conditions at nozzle exit.

2. The nozzle is underexpanded i.e. expansion fan emanates from the nozzle lip at the nozzle exit.

3. The flow field is considered inviscid (we do have highly viscous region of very thin shock wave which is of the order of 10^{-5}cm and viscous dissipation near base).

4. The flow field is non-reacting i.e. frozen flow and the exhaust gases are calorically perfect i.e. γ is not the function of temperature.

5. **The trailing shock wave is oblique in nature and pressure post trailing shock wave is equal to the pressure at the inflection point.**

3.4 Working of preliminary model

Based on supersonic area ratio (AR = 12) of the bell nozzle and gamma value ($\gamma = 1.15$) for the exhaust gases, Mach number (supersonic) at nozzle exit is calculated. The static pressure at nozzle exit, p_j is calculated based on chamber pressure $p_{chamber}$. This is done by considering the flow inside the nozzle to be isentropic from the chamber to the nozzle exit. The flow inside the nozzle is referred to as internal flow and the flow field outside the nozzle is considered as external flow field. Since the initial input to the model is pressure, p_j and Mach number, M_j at nozzle exit, the change in gamma value in the internal flow field will simply simulate different cases with different p_j and M_j as input to the proposed model.

3.4.1 Calculation of M_j and p_j

The Mach number at nozzle exit can be calculated based on equation (3.1). The left hand side of the equation (3.1) i.e. A/A^* which represents the area ratio of the nozzle. If the sonic area i.e. A^* is equal to area of throat, A_t, we can use equation (3.1) to calculate the value of M_j at the nozzle exit.

$$\frac{A}{A^*} = \left(\frac{\gamma+1}{2}\right)^{-\frac{\gamma+1}{2(\gamma-1)}} \times \frac{\left(1+\frac{\gamma-1}{2}M_j^2\right)^{\frac{\gamma+1}{2(\gamma-1)}}}{M_j} \tag{3.1}$$

Figure 3.3 shows the variation of Mach number with respect to area ratio. The plot has been generated by implementation of equation (3.1) in a python code. We can observe there are two values of Mach number for a single area ratio, this is because the equation (3.1) is quadratic in M for a fixed area ratio. So, we can expect two roots of equation (3.1). A green dashed horizontal line (M = 1) demarcates the subsonic and supersonic regions.

We obtain M_j (supersonic) from the given area ratio, i.e. A_e/A_t at nozzle exit using equation (3.1). We then use isentropic relations (since the internal flow field is assumed to be isentropic) as shown in equation (3.2) to calculate the nozzle exit pressure, p_j.

$$\frac{p_{chamber}}{p_j} = \left(1 + \frac{\gamma - 1}{2} {M_j}^2\right)^{\frac{\gamma}{\gamma - 1}} \tag{3.2}$$

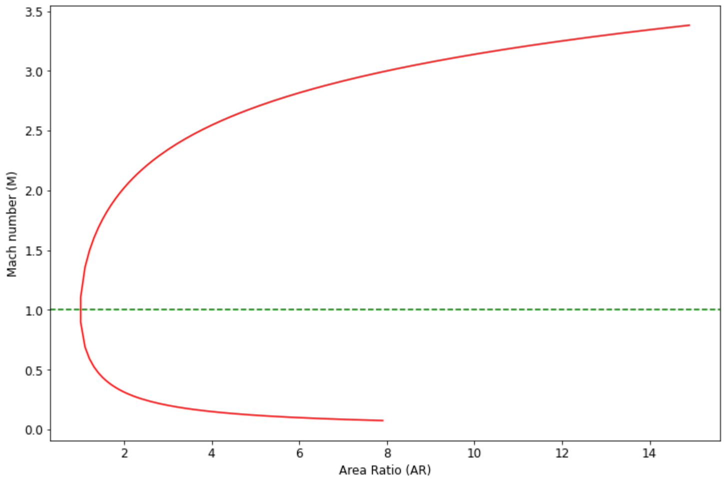

Figure 3.3: Area ratio vs Mach number

Now, we have the input parameters M_j and p_j to the model. We shall first discuss the flow chart and then take up each stations one by one.

3.4.2 Flow chart of preliminary model

Figure 3.4 shows the flow chart for the analytical model. The model commences with p_j and M_j which we have already calculated in section 3.4.1. We perform the following steps:

1. The Mach number, M_s at the tail of expansion fan is calculated by assuming $p_s = p_\infty$. The process is isentropic in nature due to the presence of expnasion fan.

2. Flow expansion angle θ_{exp} is calculated by plugging M_s and M_j in Prandtl Meyer function, $\nu(M)$ for expansion fan.

3. We proceed to calculte the shock angle, β_{shock} with the help of $\theta_{exp} - \beta_{shock} - M_s$ relation for oblique shock wave.

4. We calculate the shock normal component of Mach number, $M_{s,n}$ with the help of M_s and β_{shock}. As we know in case of oblique shock wave, the tangential component of the velocity is conserved. The normal shock wave relations are utilized to calculate pressure post shock wave, p_{tr} with the help of $M_{s,n}$ and p_s.

5. p_{tr} is equated to inflection point pressure p_{infl}.

6. We now calculate the sonic point pressure, p^* where Mach number is equal to 1.

7. Lastly, a suitable β' factor is multiplied to sonic point pressure to obtain pressure at base p_b.

The major stations are as follows:

1. Expansion fan at nozzle exit

2. Trailing shock wave due to multi-jet interaction

3. Inflection point

4. Sonic point

5. Rocket base

3.4.3 Expansion fan

The pressure and Mach number at head of the expansion fan is p_j and M_j and at tail we have M_s and p_s respectively. We head on to calculate M_s by assuming $p_s = p_\infty$.

Calculating Mach number, M_s at tail of the expansion fan

Since, we know the fact the flow undergoes isentropic expansion with the help of expansion fan. So, the total pressure is conserved across the expansion fan. The equation (3.3) is implemented to calculate M_s as we know p_j and M_j from section 3.4.1 and p_s is assumed to be equal to ambient pressure p_∞.

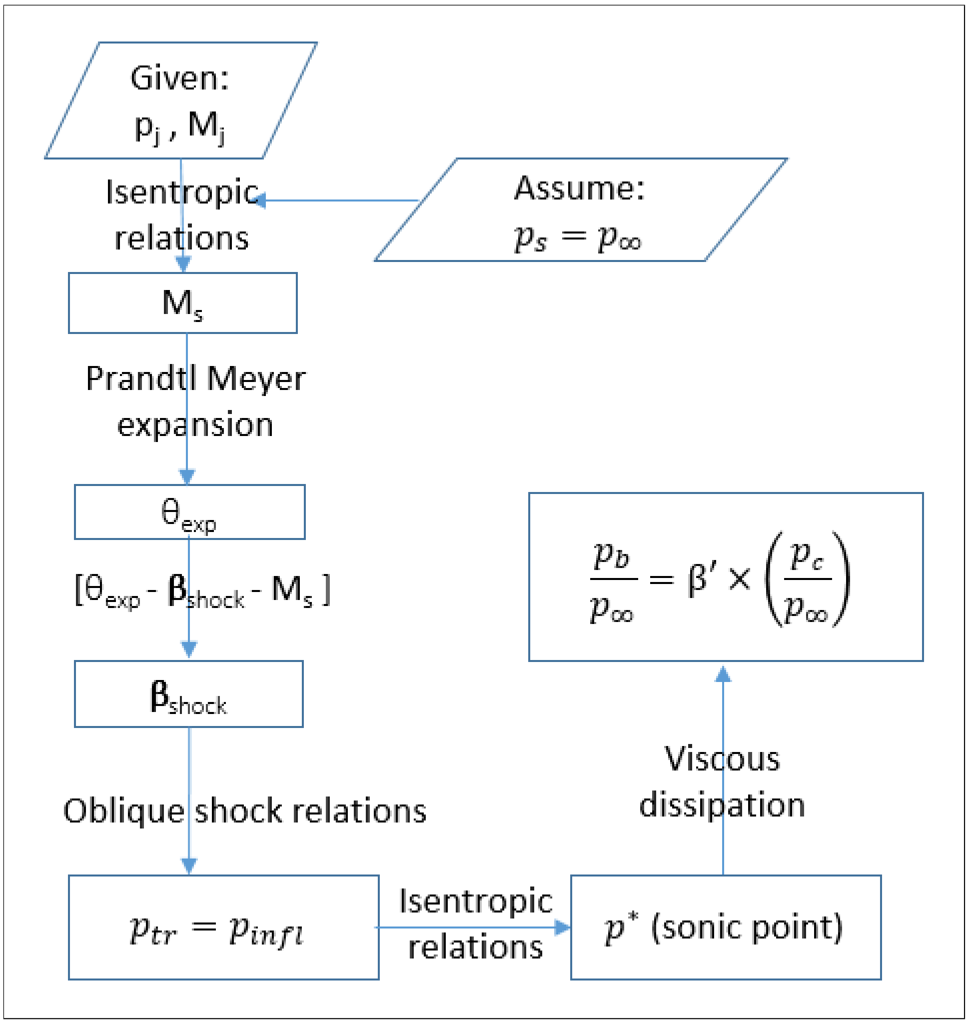

Figure 3.4: Flow chart for preliminary model

$$\frac{p_s}{p_j} = \left(\frac{1 + \frac{\gamma-1}{2} M_j^2}{1 + \frac{\gamma-1}{2} M_s^2} \right)^{\frac{\gamma}{\gamma-1}} \tag{3.3}$$

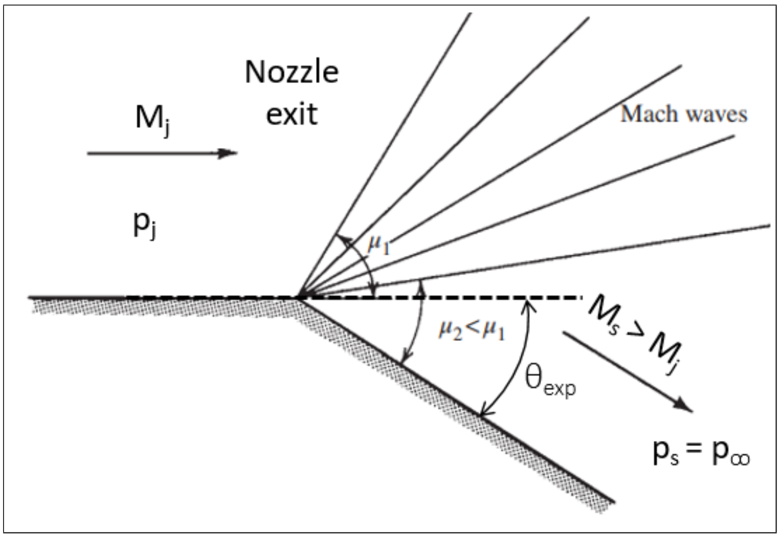

Figure 3.5: Expansion fan emanating from nozzle lip at nozzle exit[7]

Finding flow deflection angle, θ_{exp}

The flow deflection angle is given by equation (3.4).

$$\theta_{exp} = \nu(M_s) - \nu(M_j) \tag{3.4}$$

We use the Prandtl-Meyer function, $\nu(M)$ represented by equation (3.5) for two Mach numbers before the expansion fan, M_j and after the expansion fan, M_s to calculate the θ_{exp}.

$$\nu(M) = \sqrt{\frac{\gamma+1}{\gamma-1}} \arctan \left[\sqrt{\frac{\gamma-1}{\gamma+1}(M^2-1)} \right] - \arctan(\sqrt{M^2-1}) \tag{3.5}$$

We need to be cautious while using the Prandtl Mayer function for M_j. It is because the M_j lies exactly at the nozzle exit. We have to decide whether to choose $\gamma = 1.15$ (internal flow field) or $\gamma = 1.40$ (external flow field). We cannot use two different values of gamma in equation (3.4) for evaluating Prandtl Meyer function i.e. equation (3.5) for M_j and M_s. In my computation, I have chosen $\gamma = 1.40$ for computing Prandtl Meyer function for both the Mach numbers.

3.4.4 Trailing shock wave

Due to multi-jet interaction, a trailing shock wave is formed. The exhaust gases that has undergone θ_{exp} deflection by expansion fan emanating at nozzle lip from their original axial direction. The trailing shock will turn the flow by the same angle along the vehicle centreline.

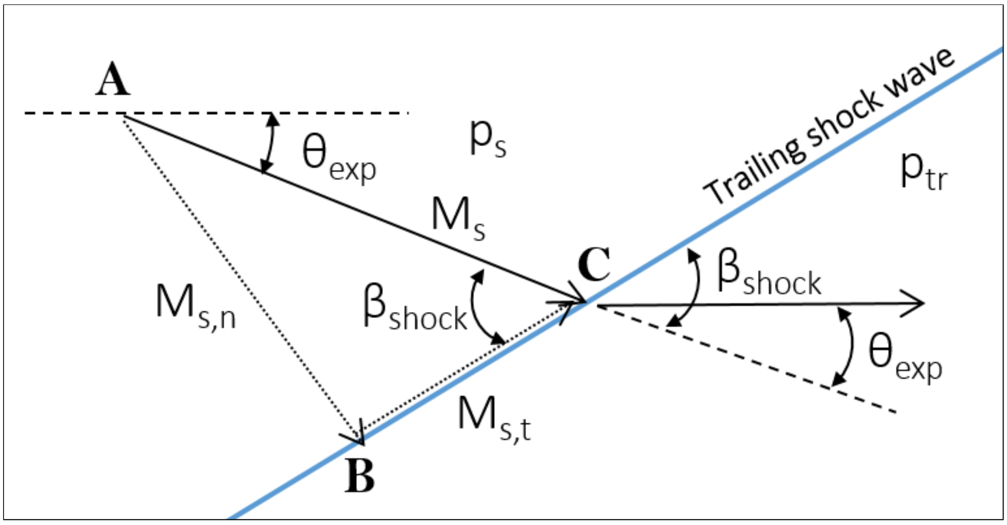

Figure 3.6: Showning $M_{s,n}$ and β_{shock}

This is a known fact that the tangential component of the velocity and corresponding Mach number $M_{s,t}$ is conserved across the oblique shock.

Calculation of β_{shock}

We make use of $\theta_{exp} - \beta_{shock} - M_s$ relation for oblique shock wave as shown in equation (3.6) to calculate β_{shock} as we know M_s and θ_{exp}.

$$\tan\theta_{exp} = 2\cot\beta_{shock}\left[\frac{M_s^2\sin^2\beta_{shock} - 1}{M_s^2(\gamma + \cos 2\beta_{shock}) + 2}\right] \tag{3.6}$$

Calculation of $M_{s,n}$

We can use ΔABC as shown in figure 3.6 to calculate the $M_{s,n}$ by using equation (3.7).

$$M_{s,n} = M_s sin\beta_{shock} \tag{3.7}$$

Calculation of p_{tr}

Now, we shall proceed to calculate the pressure post trailing shock wave, p_{tr} using $M_{s,n}$ and p_s using (3.8)

$$\frac{p_{tr}}{p_s} = 1 + \frac{2\gamma}{\gamma+1}(M_{s,n}^2 \sin^2 \beta_{shock} - 1) \tag{3.8}$$

3.4.5 Inflection point

We equate the p_{tr} to p_{infl} to obtain inflection point pressure.

$$p_{infl} = p_{tr} \tag{3.9}$$

3.4.6 Sonic point, p^*

In order to calculate the sonic point pressure, p^* , can make use of equation (3.10).

$$\frac{p_{infl}}{p^*} = \left(1 + \frac{\gamma-1}{2}M^2\right)^{\frac{\gamma}{\gamma-1}} \tag{3.10}$$

If we substitute $M = 1$ in the equation (3.10), it reduces to equation (3.11).

$$p^* = p_{infl}\left(\frac{2}{\gamma+1}\right)^{\frac{\gamma}{\gamma-1}} \tag{3.11}$$

So, we can calculate the p^*.

3.4.7 Rocket base, p_b

Finally, the rocket base pressure is calculated using a suitable factor β' known as viscous dissipation factor as given by equation (3.12).

$$p_b = \beta' p^* \tag{3.12}$$

3.5 Semi-analytical model

As we know, the mult-jet interaction flow field is a complex. There are several flow structures like expansion fan, shear layers and shock waves interacting with each other. In the preliminary model, we have introduced viscous dissipation only in the final step for calculating the base pressure. There is no much ground to justify, why we choose a certain value of β'. So, in order to get a further insight into the flow field physics, we turn our attention towards CFD simulations. The sole purpose of CFD simulation is to bring out a certain numerical factor/s that can be utilized in the model to accommodate the viscous effects. So, two test case NPRs i.e. 990 and 3760 are chosen as lower and upper bounds. The improvised model will predict the pressure at the rocket base centre at all other intermediate NPRs within the bounds.

3.5.1 Assumptions of semi-analytical model

Some of the assumptions of the preliminary model were upgraded based on insights provided by CFD simulations.

1. The post trailing shock wave pressure, p_{tr} is multiplied by an α factor to gain inflection point pressure, p_{infl}. The alpha factor is discussed in detail in chapter on results. The α factor is obtained from post processing of CFD simulation which accounts for viscous effects present between the nozzle exit and the inflection point.

2. A β' factor is multiplied to inflection point pressure, p_{infl} to obtain pressure at rocket base centre, p_b. This β' factor accounts for total pressure loss between the two stagnation points viz. inflection point and point at base centre.

Flow chart of semi-analytical model

The p_{tr} is obtained as explained in inviscid part of the preliminary model. The flow chart for semi-analytical model is as shown in the figure 3.7.

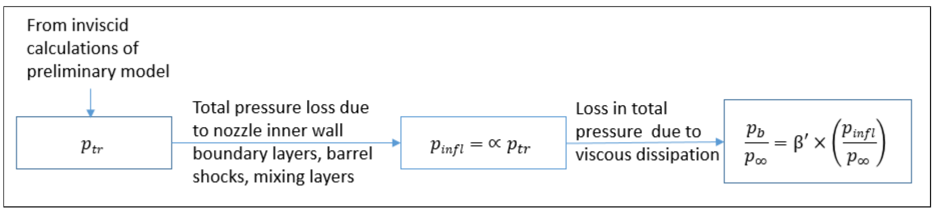

Figure 3.7: Flow chart of semi-analytical model

3.6 Summary of semi-analytical model

The model takes nozzle exit conditions, M_j and p_j as input parameters. By using isentropic relations, Mach number M_s at the tail of expansion fan is calculated by assuming $p_s = p_\infty$. The flow deflection angle, θ_{exp} is computed with the help of Prandtl Meyer function evaluation for M_j and M_s. Based on $\theta_{exp} - \beta_{shock} - M_s$ relation, we get to know β_{shock}. The pressure post trailing shock wave, p_{tr} is calculated based on M_s and β_{shock}. An α factor is multiplied to p_{tr} to get inflection point pressure, p_{infl}. Lastly, the base pressure, p_b is calculated by multiplying p_{infl} by the viscous dissipation factor, β'.

Chapter 4

CFD Data Analysis

The experimental results from Musial and Ward [4] provide base pressure distribution data only at the base plate.Among various configurations, the base pressure distribution data corresponding to configuration 1b ($D_s/D_e = 2.18$ and $L/D_e = 0.7015$) for the bell-shaped nozzle has been chosen. It is because the nozzle extension ratio for this configuration is moderate and a practical case when compared to configurations 1a ($L/D_e = 1.7326$) and 1c ($L/D_e = 0.0425$). A 3D simulation was performed by Pratikkumar Raje (Ph.D. scholar of Hypersonic CFD Lab) using his own SUQ-SST turbulence model to solve the RANS equations. The simulations were conducted for two NPR cases i.e. 990 and 3760 of configuration 1b. Further post-processing of results were carried out.

4.1 Extraction of pressure and Mach number data along limiting streamtraces

In order to make the proposed semi-analytical model more robust, we need to probe into the details of the flow field. In the model, the pressure and Mach number data are available at a particular points in the flow field. While it comes to CFD, various data points are available in computational domain. In order to recognize the flow features like expansion fan and trailing shock wave as depicted in model, we need to extract data along a particular streamtace. By doing so, we can compare the pressure at the tail of expansion fan against model predictions. This tells us whether there is only expansion going on or any other viscous effects are also in play simultaneously. Now, we should decide which streamtrace to choose.

If we fix the inlet Mach number as $M = 1.02$ for streamtrace originating at $z/D_b = 0.17$ (x-axis) and $y/D_b = -0.12$ (y-axis), then for higher NPR the

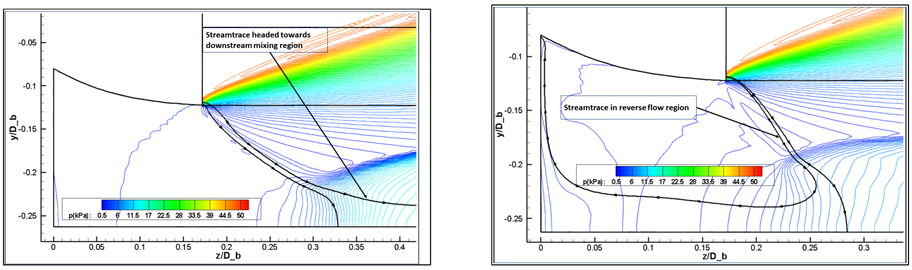

(a) NPR = 990 (b) NPR = 3760

Figure 4.1: Pressure contours showing streamtraces in downstream flow region and in reverse flow regions for two different NPR cases

streamtrace was found to be in reverse flow region near the base while that of lower NPR it was found to be in downstream mixing region as depicted in the figure 4.1.

The above issue can be resolved if we choose a streamtrace that neither lies in reverse flow region nor in downstream mixing region. Hence, a very specific streamtrace called limiting streamtrace which demarcates the reverse flow region and the downstream flow can be picked for extracting the values of pressure and Mach number.

The contours of Mach number for both the NPR cases show the various flow structures present in the flow field. The limiting streamtrace at lower NPR seems to go through expansion fan emanated from nozzle lip, barrel shock wave, free shear layer and trailing shock wave. But in case of higher NPR, the limiting streamtrace only goes through expansion fan, shear layer and trailing shock wave. It does not passes through barrel shock wave.This is shown in Mach contours of figures 4.3 and 4.2.

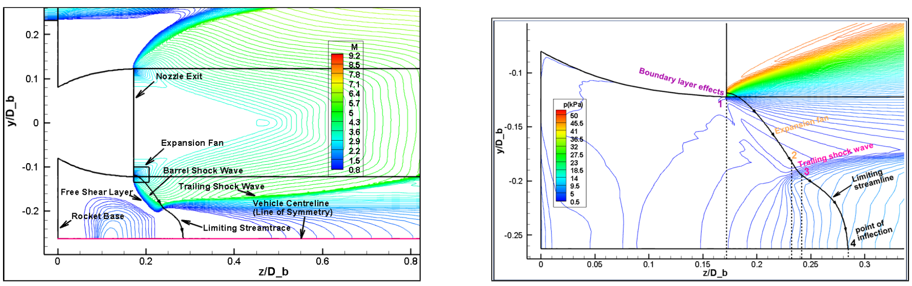

(a) Mach contour (b) Pressure contour

Figure 4.2: Showing flow features and limiting streamtrace and marking of various zones on it for NPR = 3760

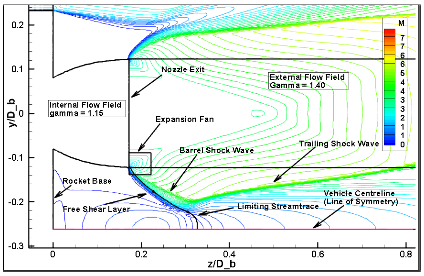

(a) Mach contour

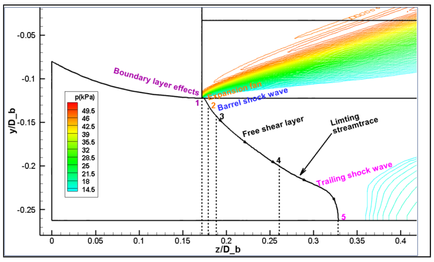

(b) Pressure contour

Figure 4.3: Showing flow features and limiting streamtrace and marking of various zones on it for NPR = 990

Figure 4.5 and 4.4 show the variation of static pressure and Mach number along limiting streamtraces for 990 and 3760 NPR cases respectively. For both the NPR cases point 1 is the nozzle exit, from point 1 to point 2 we can observe the flow expansion via Prandtl Meyer expansion fan. For NPR = 990, we can observe there is a constant pressure region from point 3 to 4 which indicates that the limiting stremtrace is in shear layer region as evident from the figure 4.3 (a). The shear layer for NPR = 3760 is not vividly visible. A pressure jump across the trailing shock wave can be observed from point 4 to 5 for lower NPR case as depicted in figure 4.5 and from point 3 to 4 for higher NPR as indicated in figure 4.4.

The values of static pressure and Mach number at point 1 is indicated by p_j and M_j respectively. The point 2 is considered as the tail of the expansion fan and p_s and M_s represent the static pressure and Mach number respectively at this point. The static pressure in the shear layer is denoted by p_{sl} and that of point of inflection by p_{infl}. The values of aforementioned variables along the limiting streamtrace is tabulated in table 4.1 for two NPR cases.

Table 4.1: Static pressure (kPa) and Mach number at various stations along limiting streamtrace in CFD for different NPRs

NPR↓ Stations →	p_j	M_j	p_s	M_s	p_{sl}	p_{infl}
990	47.4	0.64	1.56	2.60	2.27	9.03
3760	47.4	1.07	0.29	4.59	-	3.85

An interesting thing to note is the location of trailing shock wave which is pushed further away from the vehicle centreline as NPR increases. This is because the increase in NPR also enhances the radial expansion of the jets and they overlap on each other earlier compared to lower NPR case forming much stronger trailing shock wave.

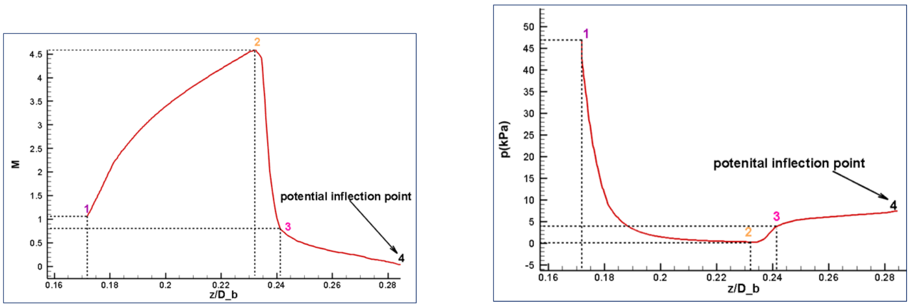

(a) Mach number (b) Static pressure

Figure 4.4: Showing variation of Mach number and static pressure along limiting streamtrace for NPR = 3760

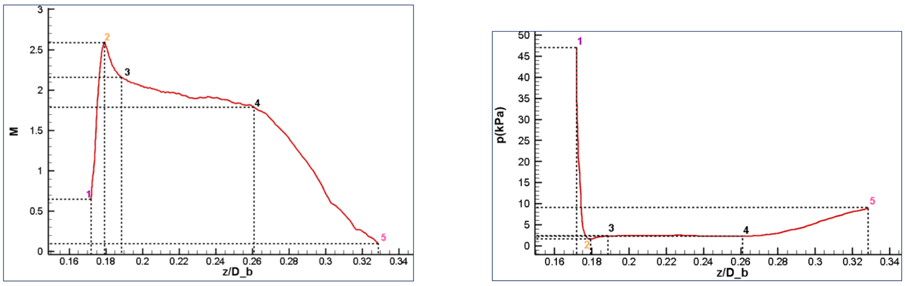

(a) Mach number (b) Static pressure

Figure 4.5: Showing variation of Mach number and static pressure along limiting streamtrace for NPR = 990

4.2 Extraction of pressure data for inflection point and base centre along vehicle centreline

The inflection point will lie on the vehicle centreline due to symmetry of the problem. Before moving to base pressure we need to figure out the pressure value at the inflection point. This is because in our semi-analytical proposed model the total pressure loss from inflection point to the base centre is encapsulated by the factor denoted by β'. So, it becomes important to know the pressure at inflection point.

One way to figure out the inflection point pressure is by following the steps as mentioned below. To elucidate, let us take a consider a case of NPR = 990.

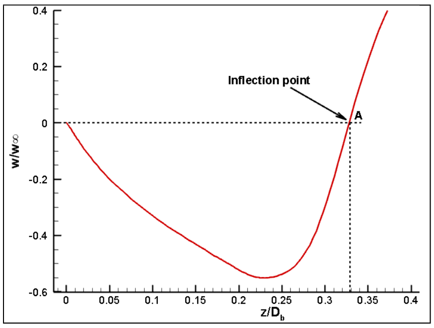

(a) Location of inflection point

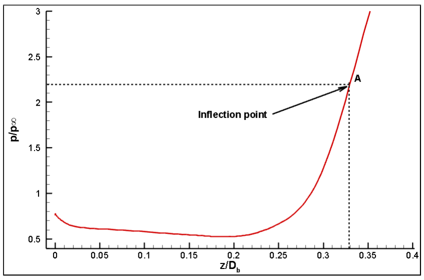

(b) Inflection point pressure

Figure 4.6: Showing inflection point and corresponding pressure along vehicle centreline for NPR = 3760

1. First of all, we plot the variations of flow field variables i.e. axial velocity component 'w' (in z-direction) and pressure along vehicle centreline. The axial velocity and pressure are normalized with corresponding freestream quantities.

2. As we know, the axial velocity of the flow is zero at the inflection point. A horizontal line is drawn in figure which indicates zero axial velocity. This horizontal line intersects with the axial velocity curve at point A. We then need to draw a vertical line that intersects with z/D_b. This gives us the location of inflection point (z/D_b location) on the vehicle centreline.

3. After we obtain the z/D_b location, we then translate this location to the pressure plot. A vertical line is drawn passing through this z/D_b location which then intersects with pressure curve. Finally, a horizontal line is drawn passing through this point that intersects the p/p_∞ axis which is the inflection point pressure.

The above procedure was followed to calculate the inflection point pressure for NPR = 3760.

The base pressure is noted at the centre of the rocket base. The base pressure is also extracted along vehicle centreline. The pressure at location $z/D_b = 0$ gives the pressure at the base centre. Since the flow stagnates on

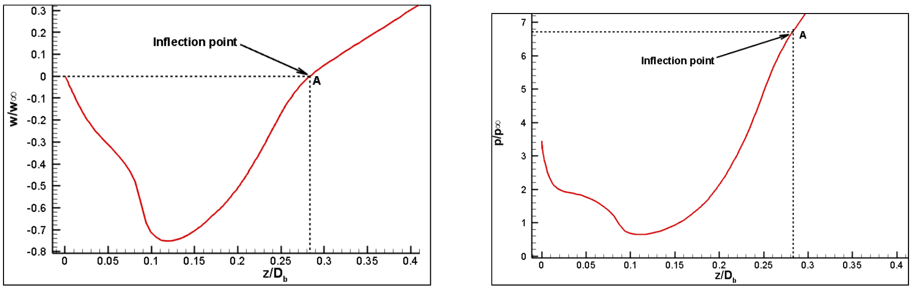

(a) Location of inflection point (b) Inflection point pressure

Figure 4.7: Showing inflection point and corresponding pressure along vehicle centreline for NPR = 3760

the base the axial component of the velocity also becomes zero. The same has been shown in figure 4.7.

The inflection point pressure, p_{infl} and its location along with pressure at base centre, p_b is tabulated in table 4.2 and is normalized with respective free stream pressure, p_∞ for two NPR cases.

Table 4.2: Pressure (kPa) values at point of inflection and base centre for different NPRs and location of inflection point along vehicle centreline in CFD

NPR	p_∞	p_{infl}	p_b	p_{infl}/p_∞	p_b/p_∞	z/D_b
990	4.18	9.16	3.26	2.19	0.78	0.33
3760	1.11	7.38	3.81	6.70	3.45	0.28

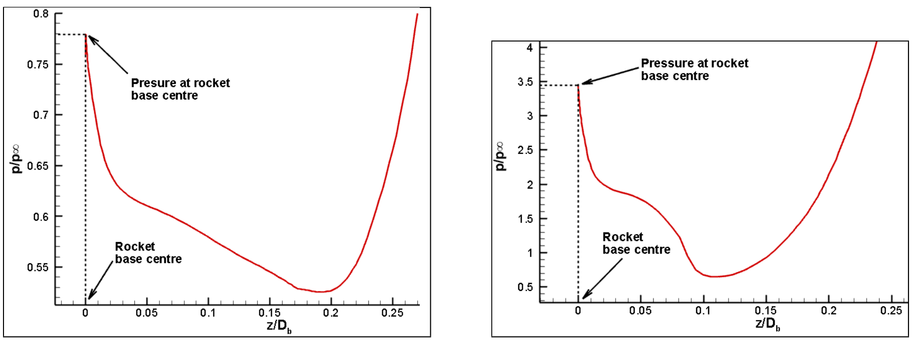

(a) NPR = 990 (b) NPR =3760

Figure 4.8: Base pressure data taken at base centre along vehicle centreline for two NPR cases

4.3 Summary

In the model, the pressure and Mach number data are available at a particular point in the flow field. But in case of CFD simulations, we have numerous data points available. If we want to observe flow phenomenon like expansion fan, formation of trailing shock wave, inflection point which are present in the proposed model. We need to divide the study in two halves. One from nozzle exit to inflection point and another from infection point to base.

A limiting streamtrace that demarcates the reverse flow region and downstream axial flow is selected for comparative study of pressure at the tail of expansion fan between the model and CFD results. This is done to understand whether flow from nozzle exit undergoes pure expansion or there is expansion with dissipation.

The extraction of data for inflection point pressure is done by identifying a zero axial velocity point along vehicle centreline and the base pressure value is chosen at the location where $z/D_b = 0$. The inflection point pressure will help in finding α that accounts for loss in total pressure between nozzle exit and the inflection point.

Chapter 5

Results and Discussions

5.1 For preliminary inviscid model

During our preliminary study, we calculated pressure downstream of the trailing shock wave using inviscid relations. Since some of the low energy gases will not be able to overcome the pressure rise downstream of trailing shock wave so they stagnate at a point called inflection point. We equated the pressure downstream of trailing shock wave to inflection point pressure. Initially, we assumed that the flow will accelerate to Mach 1 i.e. sonic point isentropically from inflection point while moving towards the base. Finally, the flow will stagnate on the base and a β' factor can be used to capture the total pressure loss due to viscous dissipation near the base. A suitable value of β' was selected to be multiplied to sonic point pressure that will give the pressure at rocket base. Figure 5.1 shows the comparison of pressure at rocket base as predicted by model for various configurations with experimental results of Musial and Ward[4].

Although the results obtained from the preliminary model was satisfactory. But there is a room for skepticism. The model predicts the base pressure so well that we may arrive at the conclusion that the base pressure is independent of geometric parameters like nozzle spacing, nozzle extension length from the rocket base etc. which is not the actual scenario. In reality, if we fix the NPR then the rocket base pressure increases with decrease in nozzle spacing and nozzle extension length. Hence, we fixed our attention to a particular geometric configuration i.e. configuration 1b because this configuration can chosen for practical purposes.

The goal of the study is to come up with numerical factor/s that can assist the inviscid model to capture total pressure loss due to viscous phenomenon so that it can predict the base pressure at intermediate NPRs for

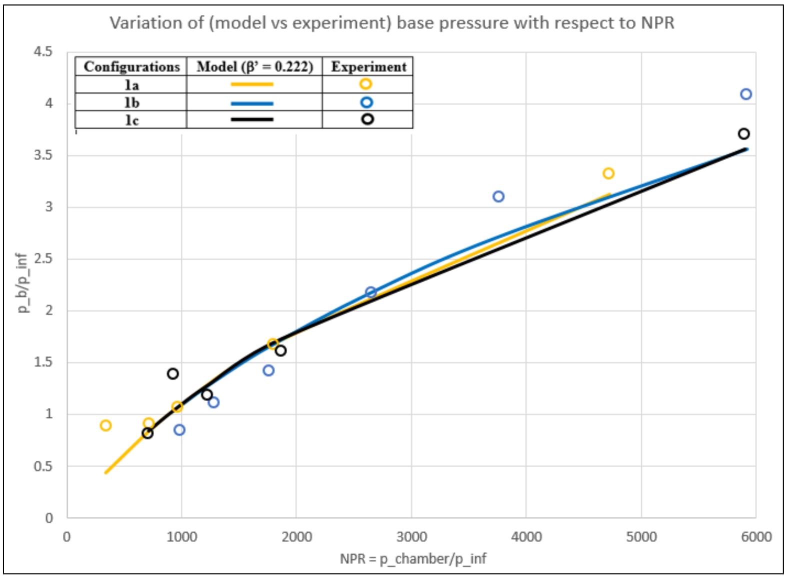

Figure 5.1: Comparison of base pressure predicted by preliminary model ($\beta' = 0.22$) with experimental data of Musial and Ward for configuration 1

configuration 1b. So, two test case NPRs i.e. 990 and 3760 were simulated to obtain meaningful numerical factors. Now, let us examine these numerical factors closely.

There are two major numerical factors that accounts for total pressure loss due to viscous interactions:

1. The alpha factor, α to compensate the loss in total pressure between nozzle exit and inflection point

2. The viscous factor, β' to account for loss in total pressure between inflection point and the base.

Let us take up α factor first.

5.2 Need for α factor

The flow stagnates at inflection point represented by point D. The post trailing shock wave pressure, $p_t r$ which is calculated by inviscid relations is much higher because we did not introduce the viscous effects when the flow moves from point A to point D as shown in figure 5.2 (a). Hence, we need an α factor to incorporate various viscous phenomenon starting from the nozzle exit to reach the inflection point. The following flow features are responsible for the total pressure loss from point A to point D.

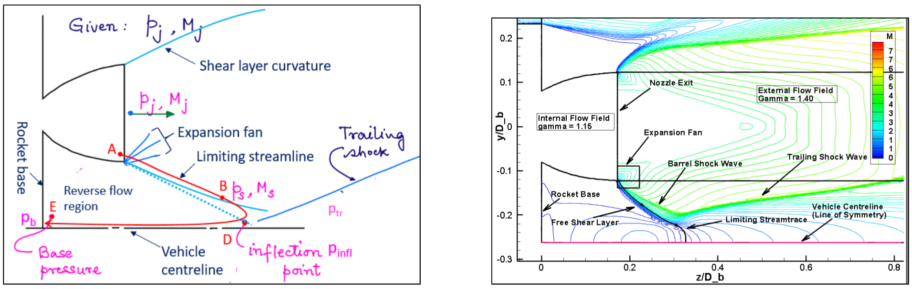

(a) Model showing various station points A, B and D along the limiting streamline

(b) Showing flow features (NPR = 990, Mach contour)

Figure 5.2: Model with major flow features vs detailed flow field as seen in CFD simulation

1. Formation of boundary layer on inner wall of nozzle
2. Jet shear layer emanating from the nozzle lip
3. Barrel shock wave embedded inside the exhaust jet
4. Formation of curved trailing shock wave
5. Shear layer curvature
6. Nozzle exit angle (bell-shaped nozzle exit angle : 3°)

5.2.1 Definition of α factor

The total pressure loss from nozzle exit i.e. point A to inflection point i.e. point D is captured by α factor. The α factor is defined as the ratio of inflection point pressure, p_{infl} which is extracted from CFD simulation to the pressure downstream of oblique trailing shock wave, p_{tr} which is obtained by inviscid calculation as described in section 3.4.2.

Mathematically,

$$\alpha = \frac{p_{infl,CFD}}{p_{tr,inviscid}} \tag{5.1}$$

We need to study the effect of the viscous flow features mentioned above on downstream trailing shock wave pressure, to identify the quantitative value of α.

5.3 Study of effect of viscous flow features on inviscid p_{tr} with the help of CFD simulations

Let us examine the inviscid pressure p_{tr} downstream of trailing shock wave more closely. Let us assume our NPR is fixed so that we can now study the frozen frame and can discuss the effect of various flow feature on inviscid p_{tr} by making use of CFD simulations.

i **Formation of boundary layer on inner wall of the nozzle**
A boundary layer is formed inside the inner wall of the nozzle which reduces the Mach number M_j at nozzle exit thereby reducing the p_{tr}. We can expect a lower inflection point pressure.

ii **Jet shear layer emanating from the nozzle lip**
The shear layer emanating from the nozzle lip will lower the total pressure as there will be viscous dissipation of momentum of the flow. This will lead to decline in p_{tr} and hence there will be drop in p_{infl}.

iii **Barrel shock wave embedded inside the exhaust jet**
A barrel shock wave is found embedded in the jet after point B and upstream of trailing shock wave. This barrel shock will adversely impact the total pressure. This will lower p_{tr} meaning the value of p_{infl} will be lessen.

iv **Formation of curved trailing shock wave**
A curved trailing shock wave is observed in the CFD simulation against our oblique shock assumption in the model. Again, there will be loss in p_{tr} and will decrease the infection point pressure.

v **Shear layer curvature**
The inviscid boundary of the under-expanded jet is consider a straight line in the model. However, there will curved shear layer and this also diminishes the p_{tr} and this will also result in lower value of p_{infl}.

The above discussion on effect of flow features on p_{tr} can be summarized in table 5.1.

From the above study, it becomes very clear that an α factor less than 1 is required to be multiplied to p_{tr} to obtain the inflection point pressure, p_{infl}. The value of α factor for two test case NPR are tabulated in table 5.2. An average value of 0.26 can be selected as α factor. The same value can

Table 5.1: Effect of various flow features on p_{tr}

Flow features	**Physical effect on inflection point pressure (IPP)**	**Effect on p_{tr}**
Nozzle inner wall boundary layer	Viscous effects (reduction of M_j) which lowers IPP	Decrease
Jet shear layer	Viscous dissipation results in loss of IPP	Decrease
Barrel shock wave	Reduction in Mach number and adversely affects IPP	Decrease
Curved trailing shock wave	Lower IPP due to loss in total pressure	Decrease
Shear layer curvature	lower flow deflection results in weaker shock implies lower IPP	Decrease
Nozzle exit angle	Flow deflected towards the centre centreline	Decrease

Table 5.2: Pressure (kPa) at inflection point and downstream of trailing shock wave at different NPRs and corresponding α factor

NPR	p_∞	p_{infl}	p_{tr}	α
990	4.18	9.16	38.95	0.24
3760	1.11	7.38	25.63	0.28

be used in the range of NPR of 990 to 3760 to predict the inflection point pressure.

We now shift our attention on the β' factor. While performing the post processing study of the simulation results for two test cases, we observe the flow is subsonic in the reverse flow region at lower NPR and is supersonic at higher NPR. The assumption of isentropic flow acceleration till sonic point in our preliminary inviscid study was not quite correct for lower NPR case. This is because of loss in total pressure via viscous dissipation. So, we need to invoke a dissipation factor known as β'. A detailed study is performed below.

5.4 Need for β'

When jets interact, the low energy exhaust gases from nozzle exit cannot overcome pressure downstream of the trailing shock wave and stagnates at a point in the flow known as inflection point as depicted in figure 5.3. Then the flow rushes towards the base instead of going downstream. This reverse flow is also called 'updraft plume'. The flow commences its journey from the inflection point towards the rocket base and may reach to supersonic Mach number before impinging on the base. The flow stagnates on the base and then leaves out radially from vent area in between the nozzles in 3D. The pressure at rocket base centre directly gets affected by the inflection point pressure. So, inflection point pressure becomes cardinal before we calculate the pressure at rocket base centre.

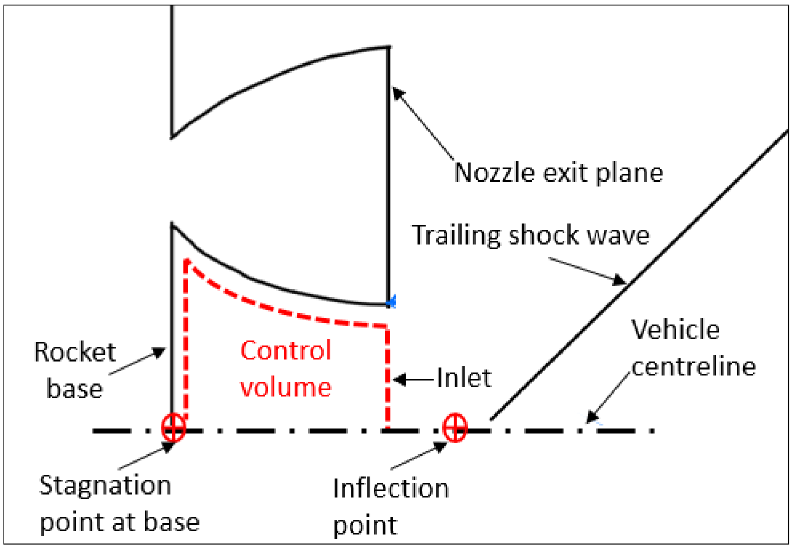

Figure 5.3: The dotted red line shows control volume (CV) bounded by rocket base and outer wall of the nozzle. The CV is symmetric about the vehicle centreline.

On the journey from inflection point to rocket base centre there will be loss in total pressure of the flow. The flow dissipates its momentum via molecular diffusion and turbulent diffusion known as viscous dissipation. We can use CFD simulations results to come up with a meaning full factor, denoted by β', that encapsulates the loss of total pressure due to viscous dissipation and presence of shocks in the flow field. In other words, we can say that β' factor less than 1 should be multiplied to the inflection point pressure and the resulting pressure is the pressure at rocket base centre.

5.4.1 Definition of β'

As we increase NPR, the inflection point pressure, p_{infl}/p_∞ increases consequently increasing the pressure at base centre, p_b/p_∞. So, we define the viscous dissipation factor, β' as follows:

$$\beta' = \frac{p_{infl} - p_b}{p_{infl}} \tag{5.2}$$

We can identify two major competing effects that cause total pressure loss as flow moves from inflection point to the base centre:

i Viscous dissipation due to molecular diffusion.

ii Presence of shock waves in the flow field.

Table 5.3: Pressure (kPa) values at point of inflection and base centre for different NPRs along vehicle centreline in CFD and corresponding β'_{cfd}

NPR	p_∞	p_{infl}	p_b	p_{infl}/p_∞	p_b/p_∞	β'_{cfd}
990	4.18	9.16	3.26	2.19	0.78	0.64
3760	1.11	7.38	3.81	6.70	3.45	0.48

We noticed the following:

1 The viscous phenomenon is more dominant at lower NPR. At lower NPR, viscous dissipation via molecular and turbulent diffusion is dominant. The pressure gradient between the inflection point and rocket base centre is low as the ambient pressure is higher. So, the flow velocity entering the CV is lower i.e. subsonic. So, there is more time available for the flow to dissipate its momentum via diffusion. Hence, the total pressure loss is higher when the flow stagnates at base. So, we have higher value of β'.

2 At higher NPR, inviscid phenomenon is prepotent. The flow has to undergo the process of acceleration and deceleration within the same CV and also a higher pressure gradient exists between the inflection point and rocket base due to lower ambient pressure. This will increase the flow velocity to supersonic speed. The time available for diffusion will not be sufficient to reduce the total pressure and a normal shock wave appears near the rocket base to abruptly decelerate the flow to zero velocity as the flow impinges on the rocket base. So, the total pressure loss in this case is lower and hence lower β'.

Since inflection point pressure data is not available from Musial and Ward[4] experiment. The inflection point pressure from CFD has been utilized to calculate the β' in case of experiment.

Table 5.4: Pressure (kPa) values near base centre for different NPRs in experiment and corresponding β'_{exp}

NPR	$p_{b,exp}$	$p_{b,exp}/p_\infty$	β'_{exp}
990	3.59	0.85	0.61
3760	3.16	2.86	0.57

In case of CFD as well, we can infer that a lower value of β' is needed to account for loss in total pressure at higher NPR and vice-versa. The normalized base pressure is slightly over predicted in simulation results when compared to experiment. So, that might be the reason for slightly different value of β'_{exp} at different NPRs. Since the variation of β'_{exp} is not relatively large we can choose an average value of β'_{exp} as 0.59. We can use this β'_{exp} as value for dissipation factor, β' in our semi-analytical model.

5.5 Final values of α and β'

We shall now utilize the values of α and β' as mentioned in table 5.5.

Table 5.5: Values of α factor and β' factor to be used in semi-analytical model

Factors	Values
α	0.26
β'	0.59

The variation of rocket base pressure with respect to NPR is depicted as shown in figure 5.4. Here, we observe nearly linear trend of variation of base pressure as predicted by the semi-analytical model. This is because the exact dependence of α and β' on NPR is not considered. However, the qualitatively trend is inline with experimental results. As we know, engineering is not the exact science rather it is a science of making useful approximations that will provide an estimate value as a solution that can serve the purpose.

The results obtained from the model calculations can be used as ballpark number for rocket base pressure that can help aerodynamics engineer to calculate and reduce base drag. In the design of thermal protection system, this pressure data can be used to calculate the stresses due to reverse flow impingement on the rocket base.

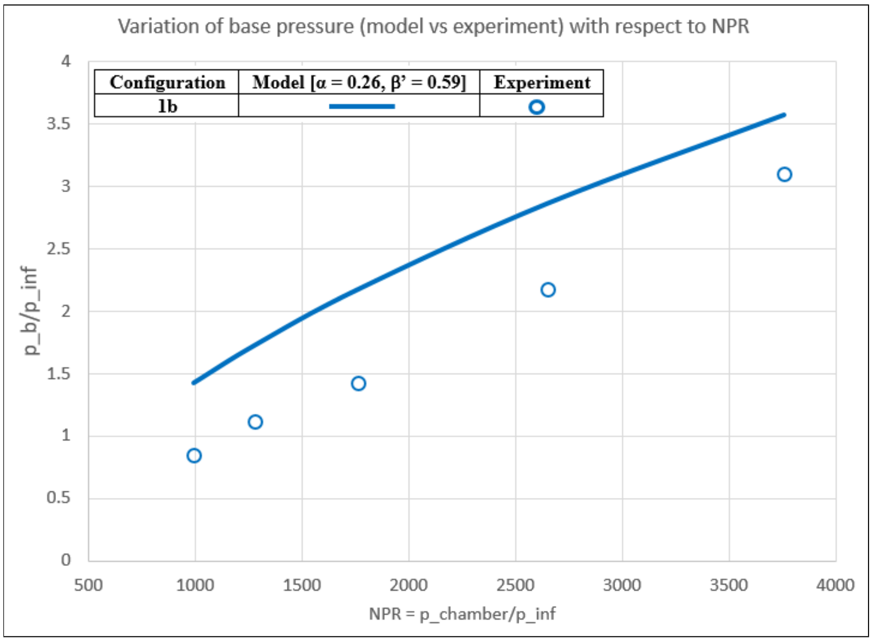

Figure 5.4: Comparison of rocket base pressure variation with respect to NPR as predicted by semi-analytical model having $\alpha = 0.26$ and $\beta' = 0.59$ with experimental data for configuration 1b (Musial and Ward)

5.6 Summary

The base pressure predicted by preliminary model is satisfactory for an arbitrary value of β'. We turned our attention to CFD simulations for two test case NPRs i.e. 990 and 3760 so that we can come up with some numerical factors that can capture the viscous effects. An α factor is used to capture total pressure loss from nozzle exit to the inflection point. Similarly, a β' factor captures the total pressure loss between the inflection point and the base. Unlike the preliminary model which over predicts the base pressure at lower NPR and vice-versa, the semi-analytical model over predicts the base pressure at all NPRs for configuration 1b. The semi-analytical model seems to approach convergence at higher NPR and divergences from experimental results as we move to lower NPRs.

Chapter 6

Conculsions and Future Work

6.1 Summary

The following are takeaways form this work on multi-jet interaction:

1 The various interactions between shocks, expansion fan and shear layers that are present in multi-jet interaction flow field make it difficult to study. Developing a pure analytical model for such a complex flow field is a challenging task. Due to multi-jet interaction, there is formation of trailing shock wave that triggers the reverse flow towards the rocket base. The exhaust gases striking the base can affect the equipment installed in base region which can lead to mission failure. Also, the base drag constitutes about 50% of total drag associated with a typical projectile travelling at Mach 0.8 with drag control[5]. It is important to study the pressure at the rocket base so that we can reduce the base drag and the stresses due to reverse flow impingement on the base. This study can also help in the design of TPS as well.

2 An attempt has been made to construct a 2D reduced order model by identifying the major flow structures associated with the reverse flow phenomenon with the help of inviscid theory. Mathematical relations related to isentropic flow, Prandtl Meyer expansion fan and oblique shock were utilized. The model has been proposed by Prof. Krishnendu Sinha.

3 The model was further improved by introducing visocus dissipation factors that can impact the inflection point pressure and base pressure. The CFD simulations for two test case NPRs i.e. 990 (lower bound) and 3760 (upper bound) are perfomed by Ph.D. scholar Pratikkumar

Raje. The post processing of CFD simulations was conducted to arrive at meaningful factors that can be incoporated in to preliminary model. This is done so that a ballpark number for base pressure can be obtained for a given NPR without doing computational intensive CFD simulations for a given geometric configuration of four nozzle cluster rocket.

4 The α factor captures the viscous effects of flow between the lip of nozzle exit (origin of expansion fan) to the inflection point (stagnation point). Similarly, β' is the viscous dissipation factor that encapsulates the total pressure loss between two stagnation points viz. inflection point and base centre when the flow moves from the inflection point to the base.

5 The improvised model with $\alpha = 0.26$ and $\beta' = 0.59$ shows nearly linear variation of base pressure with respect to NPR and slightly over predicts the base pressure when compared to experimental results of Musial and Ward.

6.2 Future work

The limitations of the model can be taken up for further study and the range of implication of the model can be improved if we can extended our study in the following manner:

1 First, the dependency of the viscous dissipation factors α and β' on NPR can be studied for a fixed geometric configuration.

2 We can further extend our model on being sensitive to various geometric parameters like nozzle extension from rocket base, nozzle spacing etc.

3 The base heat transfer study can be performed by introducing temperature at nozzle exit that can help in designing of thermal protection system.

Appendix A

Experimental base pressure data

In order to validate the model, the experimental data from NASA technical note D-1093 has been used[4].

A.0.1 Procedure

The base pressure values at radial location $r/r_b = 0.13$ (right side of $r/r_b = 0$) have been selected for configuration 1a, 1b and 1c. The base pressure value at this location for configuration 1b is either close to or higher compared to the value at $r/r_b = 0.07$ which is close to base centre location. The same has been marked by the red dots as shown in figure A.1, figure A.2 and figure A.3. The base pressure value for configuration 1b at $r/r_b = 0.13$ is listed in table A.1

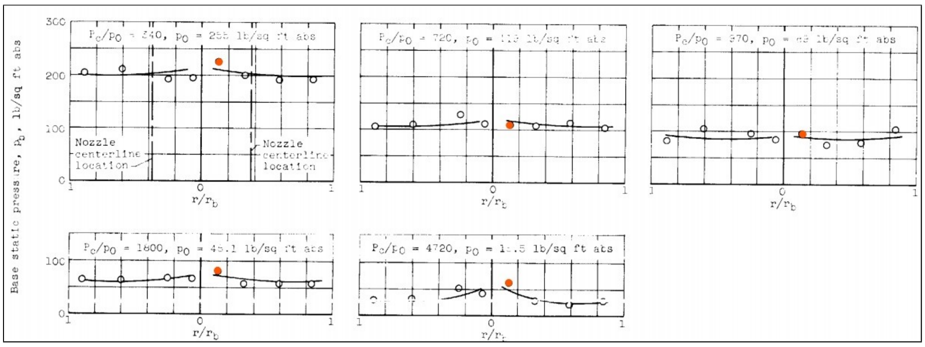

Figure A.1: Base pressure distribution for configuration 1a ($D_s/D_e = 2.18$ and $L/D_e = 1.7326$)[4]

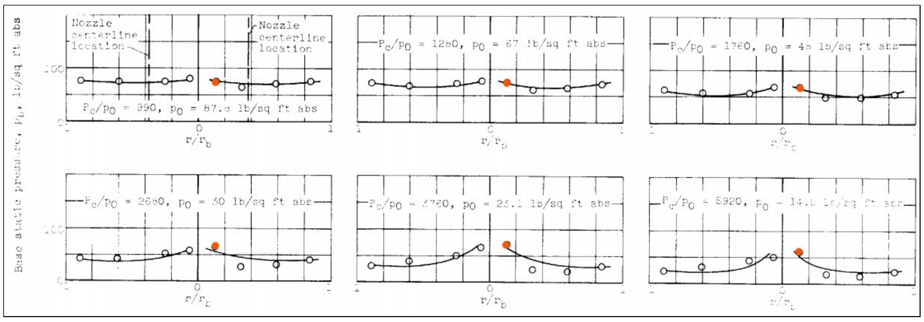

Figure A.2: Base pressure distribution for configuration 1b ($D_s/D_e = 2.18$ and $L/D_e = 0.7015$)[4]

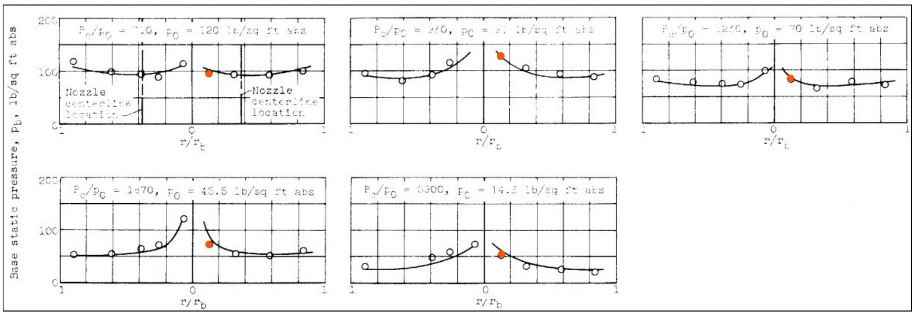

Figure A.3: Base pressure distribution for configuration 1c ($D_s/D_e = 2.18$ and $L/D_e = 0.0425$)[4]

Table A.1: Experimental base pressure value at $r/r_b = 0.13$ for configuration 1b

NPR ($p_{chamber}/p_\infty$)	990	1280	1760	2650	3760	5920
p_∞ (Pa)	4203.86	3207.96	2298.24	1436.40	1106.03	694.26
Base pressure (Pa)	3559.50	3577.31	3266.90	1524.80	3427.00	2837.14

Bibliography

[1] SLN Desikan, B Murugan, K Srinivasan, and S Sajan. Twin jet interaction and reverse flow. *Journal of Spacecraft and Rockets*, 52(6):1577–1585, 2015.

[2] Daniel Hoffpauir. New approaches to refining the launch vehicle buffet environment. `https://www.nasa.gov/offices/nesc/articles/new-approaches-to-refining-the-launch-vehicle-buffet-environment.html`, 2020.

[3] Manish Mehta, Francisco Canabal, Scott B Tashakkor, and Sheldon D Smith. Numerical base heating sensitivity study for a four-rocket engine core configuration. *Journal of Spacecraft and Rockets*, 50(3):509–526, 2013.

[4] Normal T Musial and James J Ward. *Base flow characteristics for several four-clustered rocket configurations at mach numbers from 2.0 to 3.5.* National Aeronautics and Space Administration, 1961.

[5] R Nallasamy, M Kandula, L Duncie, and P Schallhorn. Base flow and heat transfer characteristics of a four-nozzle clustered rocket engine: Effect of nozzle pressure ratio. *American Institute of Aeronautics and Astronautics*, page 35, 2011.

[6] Pratikkumar V Raje and Krishnendu Sinha. Three-dimensional simulation of rocket nozzles with multi-jet interaction using shock-unsteadiness model. In *AIAA Aviation 2019 Forum*, page 3322, 2019.

[7] Robert D Zucker and Oscar Biblarz. *Fundamentals of gas dynamics.* John Wiley & Sons, 2019.